Utrecht University

Insight Into Sparse Autonomous Seismic Acquisition With Compressive Sensing and Gradients

Earth Structure and Dynamics

Master's Thesis

Badr Almalki

Supervisor: Dr. Ivan Pires de Vasconcelos

May 2023

1 Abstract

Technological advancements in different scientific fields may allow seismic acquisition to be fully autonomous. Due to the high cost, it is still not plausible for this technology to be used. Autonomous marine seismic acquisition requires many expensive platforms and vessels to acquire high-quality seismic data. A straightforward way to reduce the cost of such seismic surveys is by using fewer platforms. However, this will result in acquiring fewer traces due to the spatial under-sampling caused by using fewer sources and receivers. This project aims to revisit new developments in compressive sensing techniques to handle missing data by reconstruction from sparse seismic data. Using data from both field and numerical settings, we looked into the role of wavefield gradients in recovering missing data from highly subsampled observations. This included experimentation with subsampling, different sparsity-promoting solvers, and the role of transformation of data to different sparse domains. The reconstruction of different datasets with their gradients using compressive sensing techniques showed promising results for regularly subsampled data. For the randomly subsampled data, the results were not as promising since the F-K domain is not an ideal sparse domain for such data.

Contents

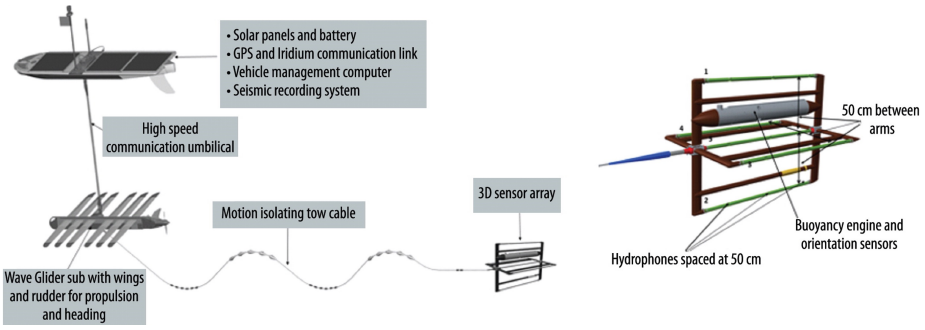

Figure 1: Autonomous marine vehicle and seismic acquisition setup (AMV), from Moldoveanu et al. [9]

2 Introduction

Marine seismic data are usually acquired by towed streamers or stationary receivers. The towed-streamer acquisition is the more widely used of the two. Many challenges face seismic acquisition, efficiency, cost, and environmental and operational issues are some of these challenges. There have been multiple studies in the field of autonomous seismic acquisition [5, 7, 9, 14, 15], which is one way to combat some of the challenges faced by seismic acquisition. The use of fully autonomous marine systems will help significantly in different fields, from oil and gas exploration to oceanographic studies. Figure 1 shows an autonomous marine vehicle that could be used for autonomous acquisition. Field experiments comparing ocean-bottom cable (OBC) data to data acquired using autonomous marine vehicles (AMV) in the Arabian Gulf [2] and the Gulf of Mexico [8]. The results of these experiments showed the potential of this new technology. Due to the high cost of this technology, it is still impractical for it to be widely used.

One way to lower the cost is by acquiring fewer data. This compression in space can be achieved by sparse spatial subsampling. Trading off coverage for a lower cost introduces another problem of missing seismic data, which can be detrimental to the whole seismic survey. Large spaces between sparsely distributed data points introduce special aliasing according to the Nyquist-Shannon theorem. The Nyquist-Shannon theorem states that the sampling rate for regularly-sampled data must be at least twice its expected frequency to produce a signal accurately and prevent aliasing [13]. To overcome these traditional constraints, reconstructing sparse irregularly-sampled data is an active field of study [10, 4]. Here, we use the concepts of compressive sensing and gradient-based reconstruction to lower the sampling rate than that required by the Nyquist-Shannon theorem. Two densely sampled datasets were used to test the gradient-based reconstruction, 2D seismic data, and synthetic ocean turbulence data, with different subsampling patterns (regular and random).

3 Compressive sensing

3.1 Compression vs compressive sensing

Both compression and compressive sensing utilize the sparsity of signals in different domains. Compression minimizes data size without lowering the quality below a specific threshold. Compressive sensing, on the other hand, is a technique used to reconstruct a signal from fewer samples than what is required by the Nyquist-Shannon theorem [6]. Compression transforms the measured data into a different domain with a sparse representation of the signal. By only keeping coefficients representing the signal and zeroing out everything else, we are left with a sparse representation of the signal. Finally, this sparse representation is transformed back into the original domain. Compressive sensing uses a similar technique, but instead of measuring the data and then throwing away what is not needed, only a fraction of the data is measured.

Compressive sensing can be achieved under two conditions, sparsity and incoherence. By sampling the data randomly, incoherence is achieved and aliasing is avoided. By transforming the signal to a basis with a sparse representation (like Fourier or Wavelet), the sparsity can be exploited to reconstruct a full signal. Figure 2 shows how keeping only 5% of the data in the Fourier domain is enough to reconstruct the original image with sufficient quality. Equations 1,2 and 3 show how the compressive sensing technique work. In equation 1, d_{mod} is a modeled densely sampled data, d_f its sparse representation in the Fourier domain, and F^H being the adjoint Fourier transform. In equation 2, the densely sampled data d_{mod} is sampled, resulting in d_{obs} with R being the restriction operator. Finally, in equation 3, the densely sampled data is substituted with its equivalent $F^H\ d_f$ and then solved for d_f.

$$d_{mod} = F^H\ d_f \tag{1}$$

$$d_{obs} = R\ d_{mod} \tag{2}$$

$$d_{obs} = R\ F^H\ d_f \tag{3}$$

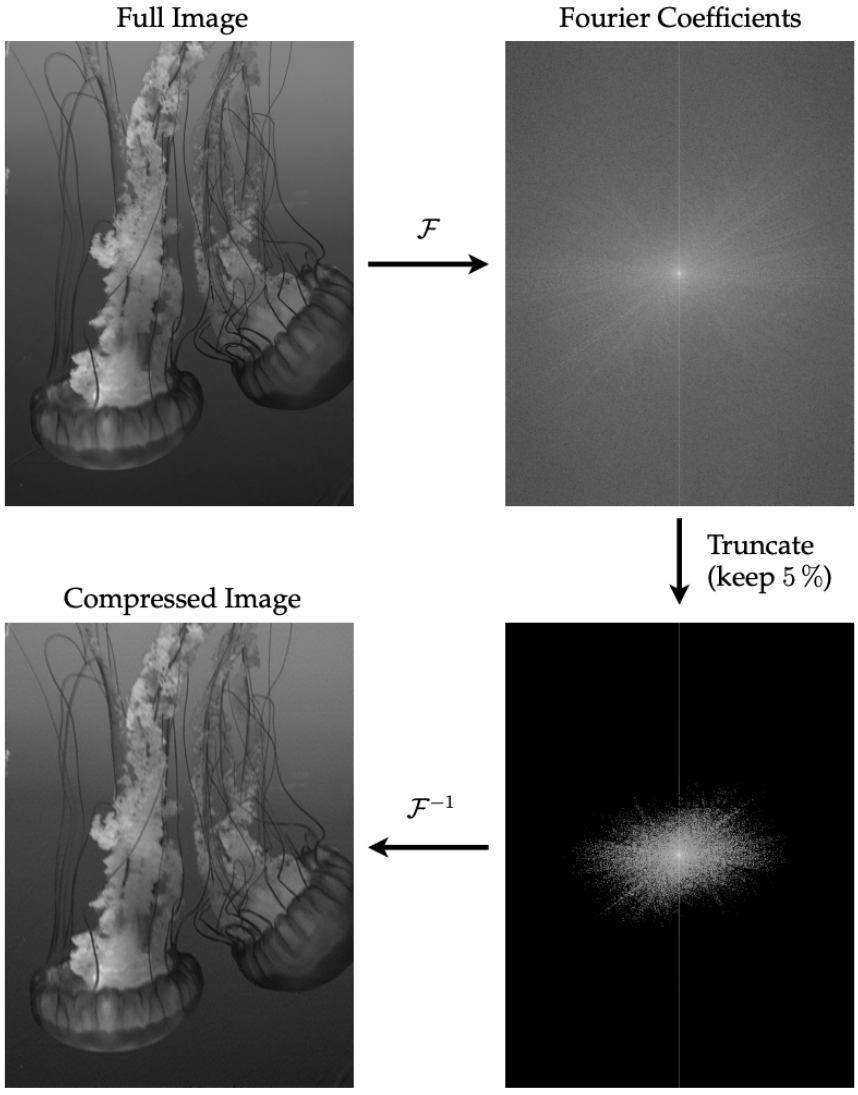

Figure 2: Compression illustration with fast Fourier transform, from Brunton and Kutz (2022) [3]

3.2 Optimization problem

Equation 3 is an inverse problem where we need to find d_f that satisfies the problem. However, there are many possible solutions making this an ill-posed problem. Equation 4 shows the optimization problem.

$$min||R\ F^H\ d_f - d_{obs}|| \tag{4}$$

Solving this problem requires more information. The constraint for this problem becomes the sparsest possible solution that is consistent with the measurements. The l_0 norm shown in equation 5 counts the total number of nonzero elements making it an indication of sparsity.

$$min||R\ F^H\ d_f - d_{obs}|| + \lambda||d_f||_0 \tag{5}$$

However, using l_0 norm as a constraint makes the problem non-convex and computationally challenging to solve. Instead, an l_1 norm is used, shown in equation 4, which calculates the sum of the absolute values. Candes-Romberg-Tao (2006) found that by minimizing the l_1 norm, the sparsest solution that satisfies the system of equations can be estimated. The solver that was chosen is the fast iterative shrinkage-thresholding algorithm (FISTA) [1].

$$min||R\ F^H\ d_f - d_{obs}|| + \lambda||d_f||_1 \tag{6}$$

As this is a large-scale inverse problem, it is not efficient to compute and manipulate matrices explicitly. Instead, these operations can be described by functions with matrix-vector products in forward and adjoint modes. Pylops [11] is an open-source python library that was used throughout this project for linear optimization.

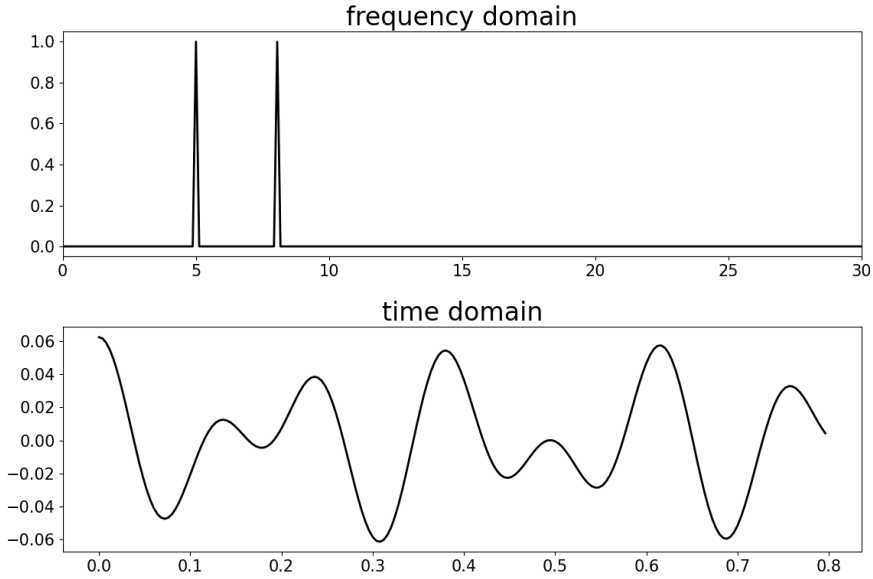

Figure 3: 1D signal in the frequency domain (top) and time domain (bottom)

4 Compressive sensing reconstruction

4.1 1D signal reconstruction

To put the compressive sensing technique into practice, we can look into a simple 1D signal and reconstruct it from under-sampled measurements. Figure 3 shows a signal in the frequency and time domains. The signal has only two frequencies, and according to the Nyquist-Shannon theorem, we need to sample it twice the highest frequency. If we under-sample it, as shown in figure 4, we can see that it is impossible to reconstruct the original signal. This is where compressive sensing shines, where it can reconstruct an under-sampled signal.

Before reconstructing the signal, we compared the effects of regular and random sampling. Figures 5 and 6 show a regularly sampled signal and its reconstruction, respectively. While figures 7 and 8 show a randomly sampled one and its reconstruction, respectively. The randomly sampled signal produced a faithful reconstruction of the original signal. The problem was solved using a sparsity-promoting solver that minimizes the L_1 norm. If a non-sparsity promoting solver was used, like least square, then the reconstruction fails, as shown in figure 9, since we want the sparsest solution possible. Figure 10 show the errors when using different regular and random sampling intervals. Random sampling gives better results, with the reconstruction being faithful when using much fewer data.

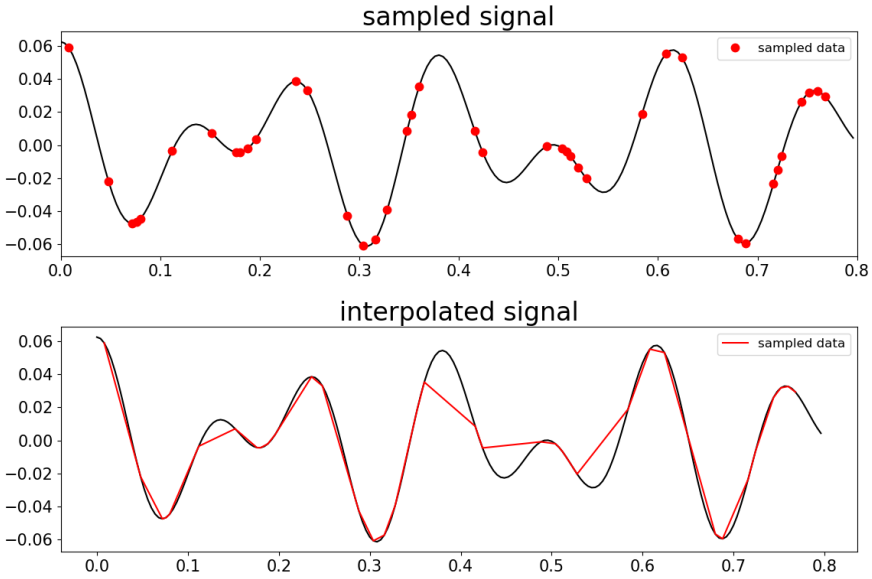

Figure 4: Sampled signal (top) and interpolated signal (bottom)

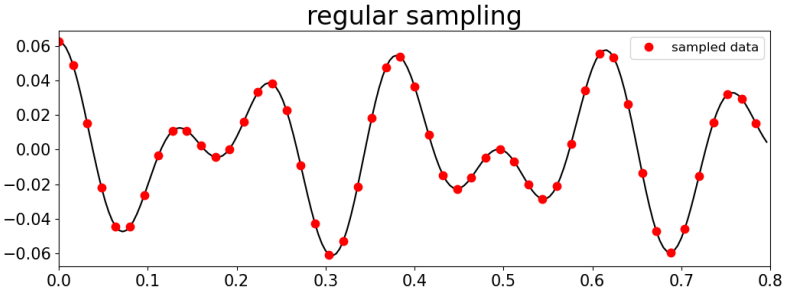

Figure 5: Regularly sampled signal

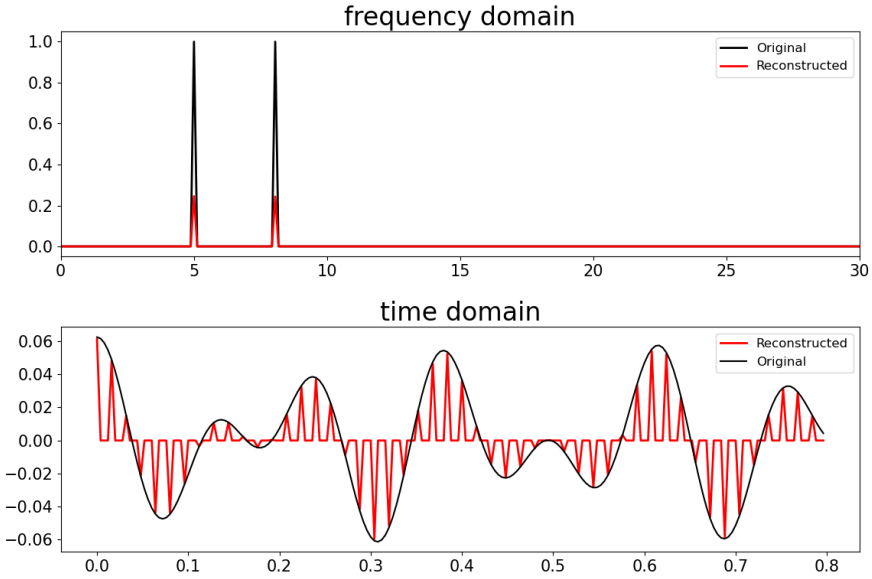

Figure 6: Reconstruction of a regularly sampled signal in the frequency domain (top) and time domain (bottom)

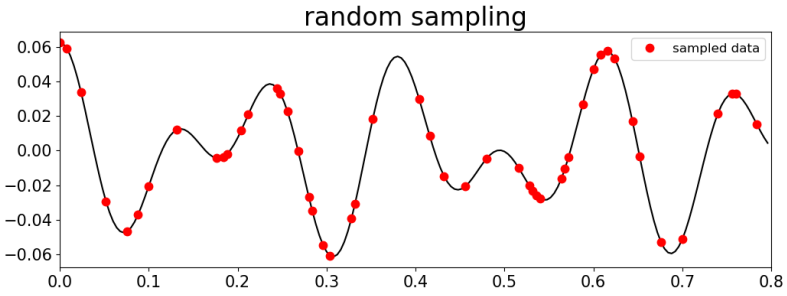

Figure 7: Randomly sampled signal

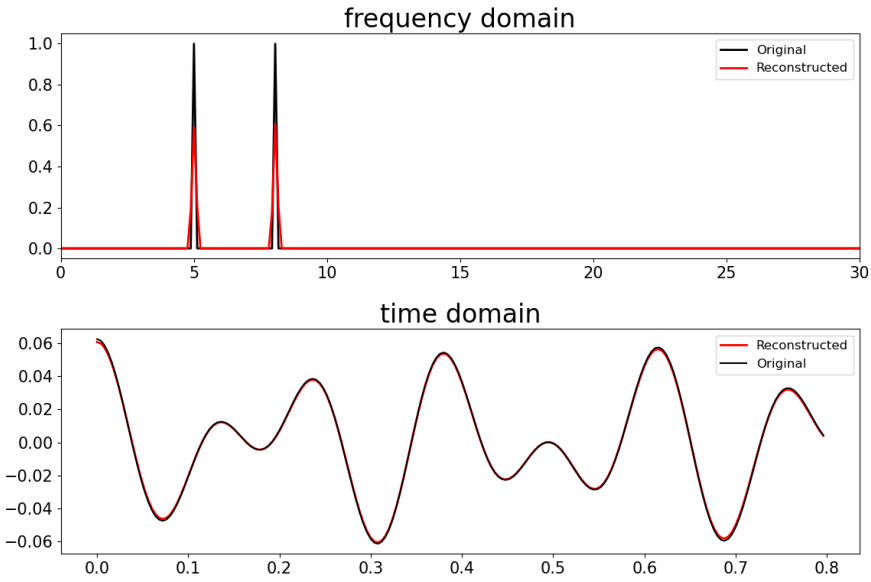

Figure 8: Reconstruction of a randomly sampled signal in the frequency domain (top) and time domain (bottom)

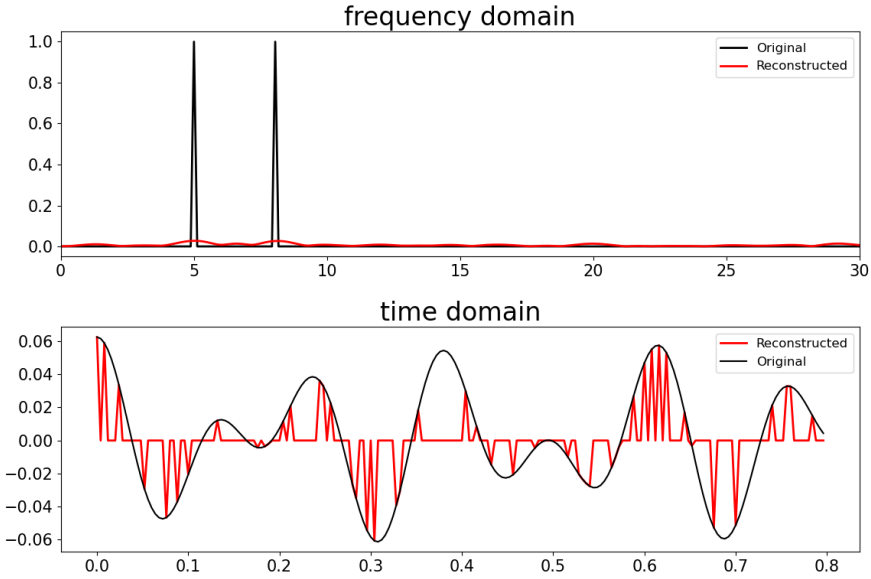

Figure 9: Reconstruction using LSQR solver in the frequency domain (top) and time domain (bottom)

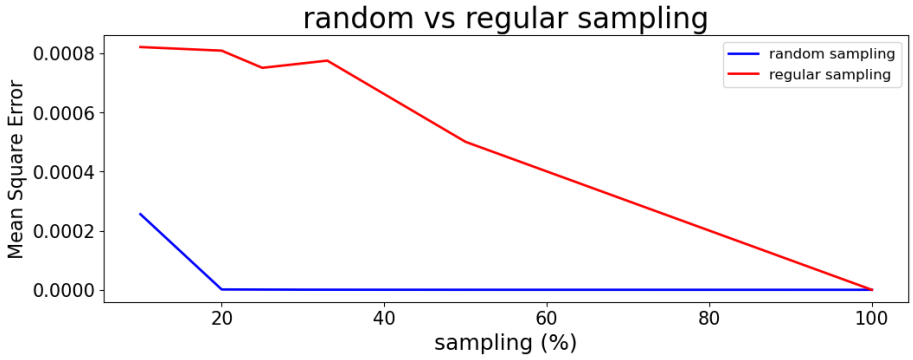

Figure 10: Regular and random sampling reconstruction errors with different sampling intervals

4.2 2D seismic data reconstruction

After showing the compressive sensing technique working on a simple 1D signal, The next step was to apply it to a real dataset. A 2D seismic data from the Gulf of Suez was chosen first. Since the data is not sparse in the time domain, it needs to be transformed into a domain with a sparse representation. In this case, it was the F-K domain. Figure 11 shows a shot gather and its equivalent in the F-K domain. Unlike the 1D signal, the 2D seismic data is not entirely sparse in the F-K domain.

4.2.1 Preconditioning

The reconstruction problem is an underdetermined system of equations. To help produce better results, a priori information is needed. A physics-based preconditioner was implemented in the F-K domain as a mask, as shown in figure 12. The dispersion in the F-K domain is estimated with a triangle shape using the constant velocity of water. By adding the F-K domain preconditioner to equation 3 mentioned before, it becomes equation 7.

$$d_{obs} = R\ P_{fk}\ F^H\ d_f \tag{7}$$

4.2.2 Regular subsampling

Figure 13 shows the data subsampled regularly using only 50% of the data. The subsampled data is transformed into the F-K domain. The data in the F-K domain show an aliasing effect due to the gaps in the data. Precondition in the F-K domain and then solve. Figure 14 shows the results, while figure 15 shows the errors using different subsampling intervals.

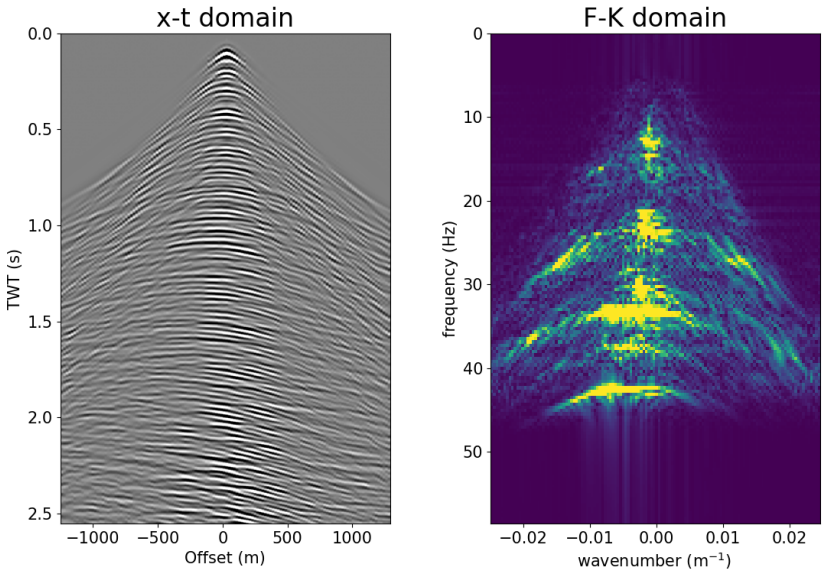

Figure 11: A shot gather in the time domain (left) and F-K domain (right)

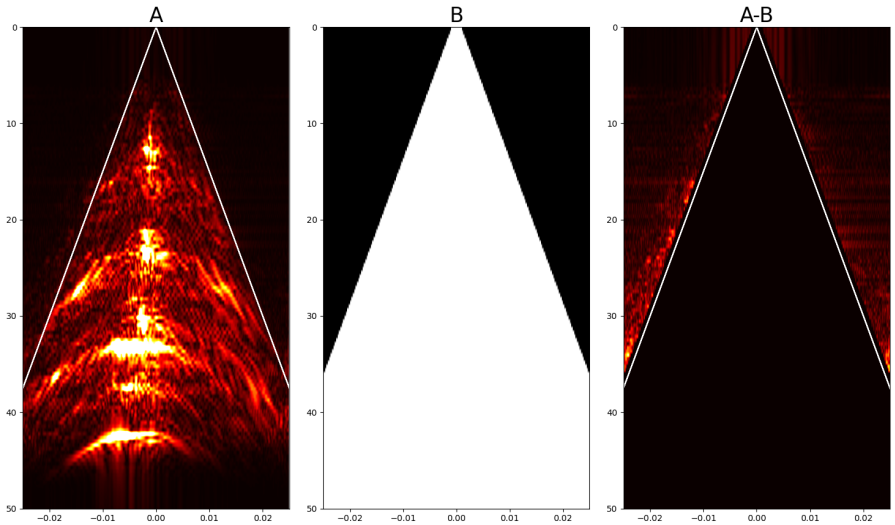

Figure 12: F-K domain preconditioning

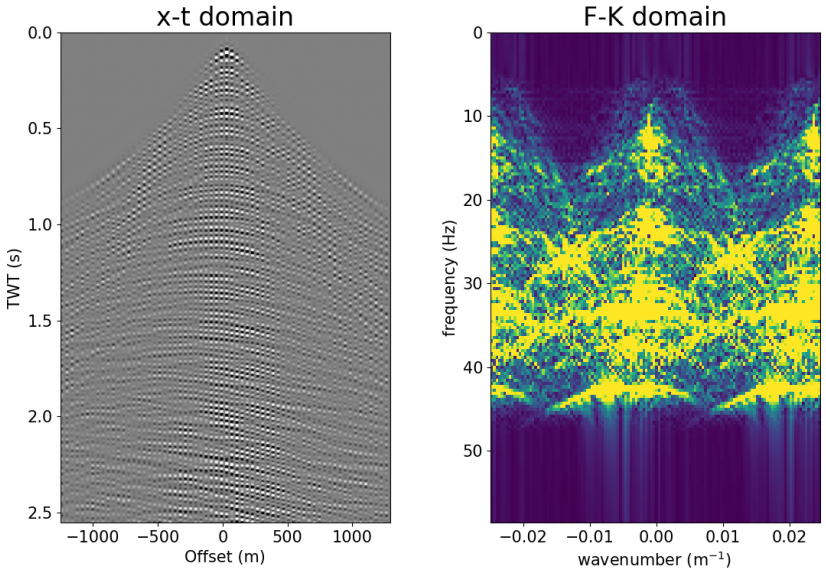

Figure 13: Regular subsampling in the time domain (left) and F-K domain (right)

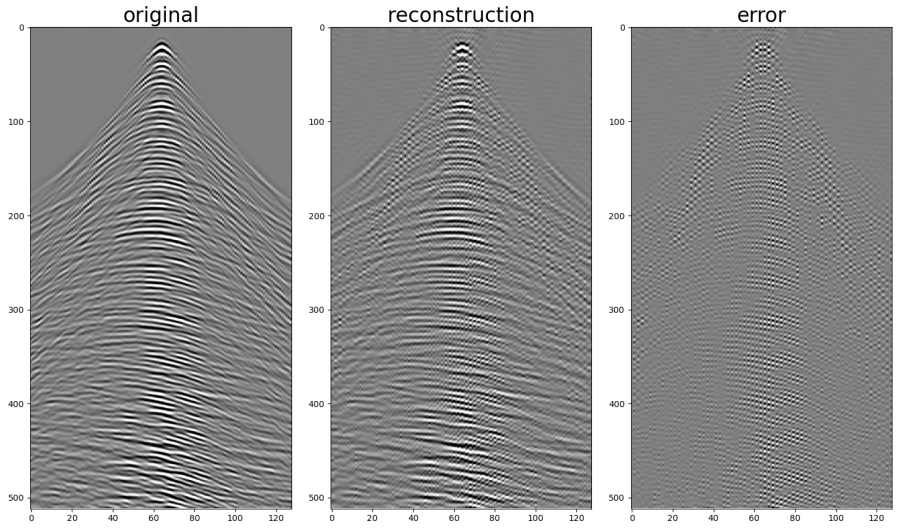

Figure 14: Reconstruction of regularly subsampled data

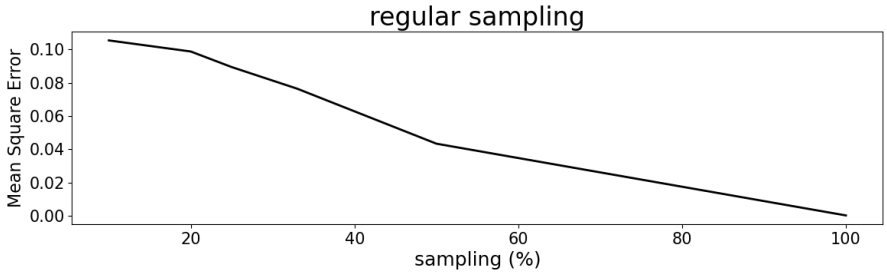

Figure 15: Regularly subsampled data reconstruction errors with different subsampling intervals

4.2.3 Random subsampling

Figure 16 shows the data subsampled randomly using only 50% of the data. The subsampled data is transformed into the F-K domain. Unlike the regularly subsampled data, the data is not aliased in the F-K domain. Figure 17 show the reconstruction results, while figure 18 shows the errors using different subsampling intervals. Comparing this to the regularly subsampled data, it produced better results using the same subsampling interval.

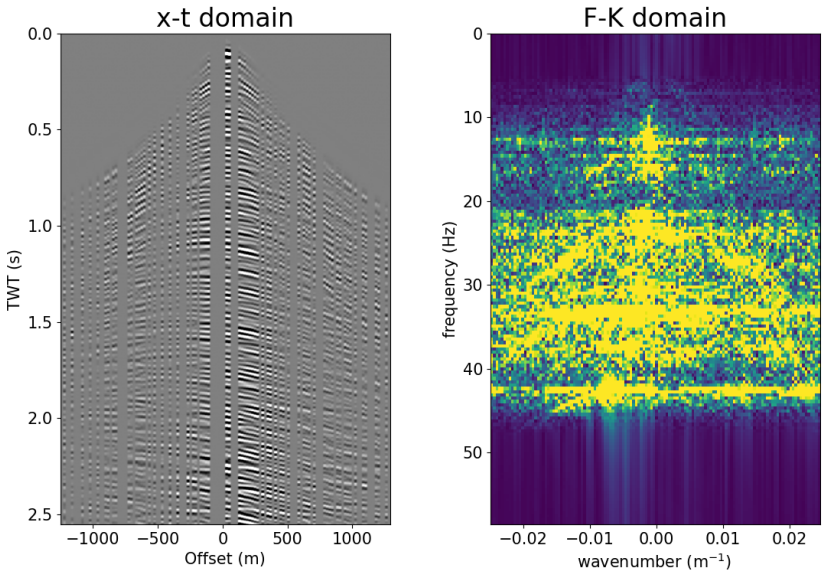

Figure 16: Random subsampling in the time domain (left) and F-K domain (right)

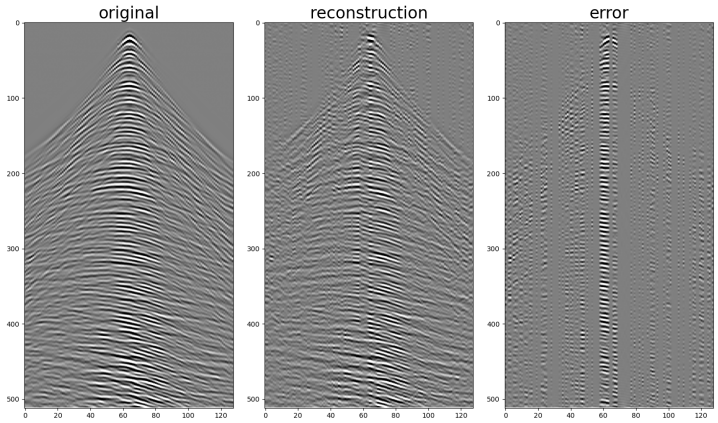

Figure 17: Reconstruction of randomly subsampled data

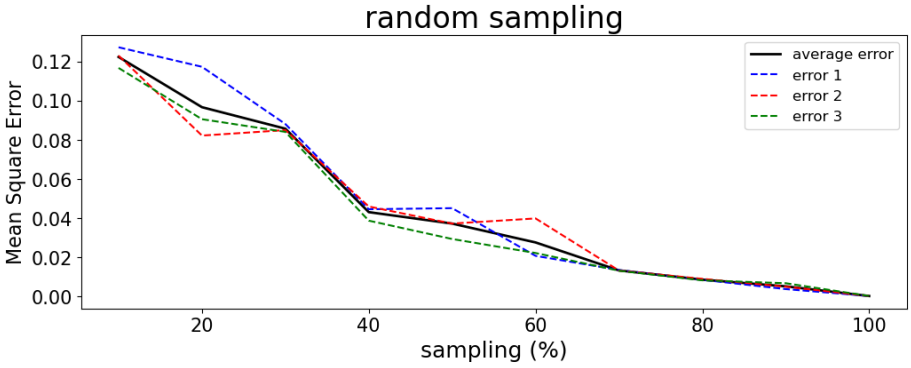

Figure 18: Randomly subsampled data reconstruction errors with different subsampling intervals

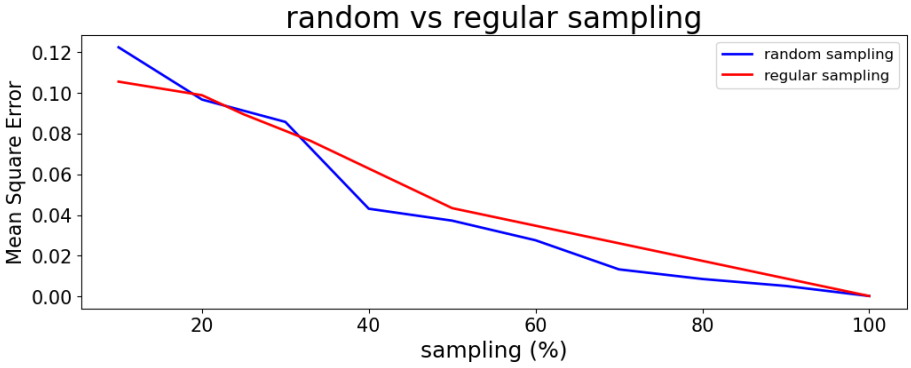

Figure 19: Comparing reconstruction errors for randomly and regularly subsampled data

5 Gradient based compressive sensing

The use of gradients of the wavefield data can further improve reconstruction using compressive sensing. Linden (1959) showed that by using the first-order gradient, the minimum sampling rate required for a faithful reconstruction is lowered by a factor of two. Robertsson et al. (2008) improved this by using both the first and second-order gradients to lower the minimum sampling rate by a factor of three. The problem with the first and second gradients becomes:

$$\begin{bmatrix} d \\ \dot{s}\dot{d} \\ \ddot{s}\ddot{d} \end{bmatrix} = \begin{bmatrix} RF^H \\ \dot{s}RF^H D_1 \\ \ddot{s}RF^H D_2 \end{bmatrix} m \tag{8}$$

$$D_1 = RF^H diag(ik_n)F \tag{9}$$

$$D_2 = RF^H diag(ik_n)^2 F \tag{10}$$

The first equation is the classical interpolation equation, and the second and third equations are for the first and second-order derivatives, respectively. d being the measured data, R the restriction operator, the inverse Fourier transform, m the desired output, and D_1 and D_2 are the operators that apply the spatial derivatives in the F-K domain. Since the derivative data may have a different range from the data d, we scale these equations on both sides so that inversion will not favor matching d over the other two datasets. Equations 9 10 are the Fourier-based models for spatial derivatives with $diag(ik_n)$ being a diagonal matrix with wavenumbers.

5.1 2D Seismic data reconstruction

The same 2D seismic dataset from the Gulf of Suez is used here again but with the incorporation of gradients. The first and second-order gradients were numerically calculated from the well-sampled dataset. However, in a real scenario, the gradient data must be measured by equipment, resulting in noisier gradient data. Figure 20 shows the first and second-order deviates for the Gulf of Suez dataset. Using the gradient data, the Gulf of Suez dataset was reconstructed by subsampling the dataset regularly and randomly.

5.1.1 Regular subsampling

Figure 21 shows the reconstruction result by regularly subsampling a third of the dataset, while figure 22 shows the error for different reconstructions using different subsampling intervals. According to these results, the reconstruction is faithful when using as low as a third of the dataset.

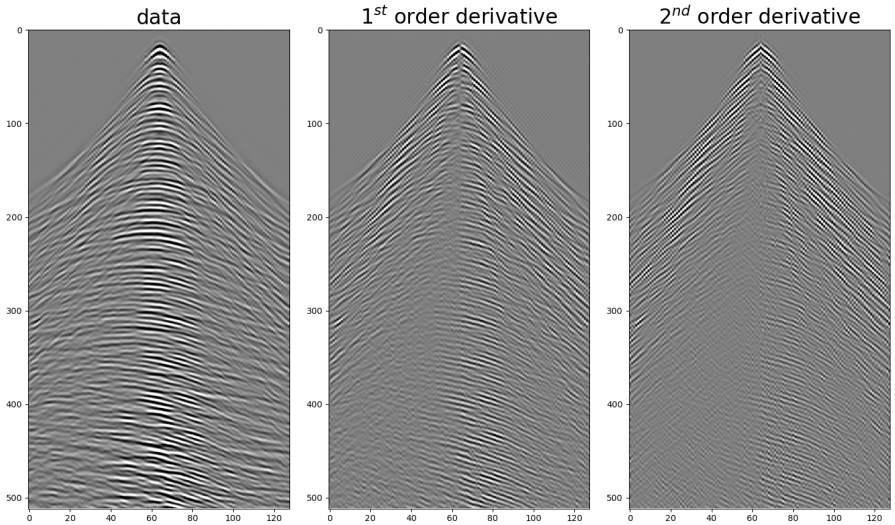

Figure 20: A shot gather with its first and second-order derivatives

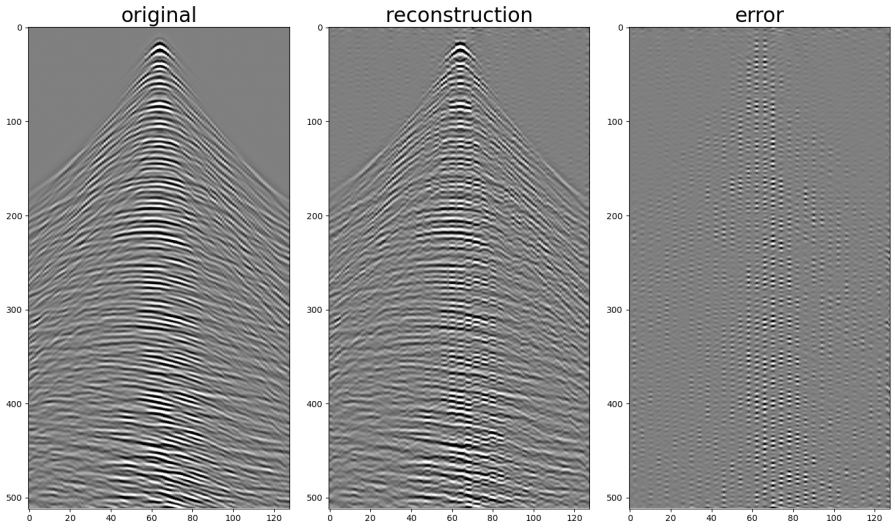

Figure 21: Reconstruction with regular subsampling

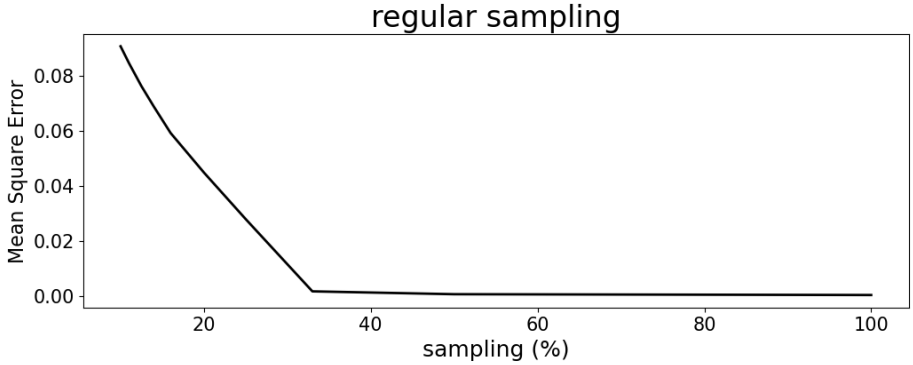

Figure 22: Regularly subsampled data reconstruction errors with different subsampling intervals

5.1.2 Random subsampling

Figure 23 shows the reconstruction result by randomly subsampling a third of the dataset, while figure 24 shows the error for different reconstructions using different subsampling intervals. Unlike the regularly subsampled dataset reconstruction, the randomly sampled dataset reconstruction is not as good.

5.2 2D synthetic ocean turbulence data reconstruction

Another dataset was used to test the gradient-based compressive sensing technique. It is a synthetic ocean turbulence dataset that was generated from a 2D ocean turbulence model (figure 26). Even though there is no contrast in the speed of waves in water, temperature and salinity variations caused by turbulence cause a contrast in the same medium. The generated data include direct arrivals and reflections from sediments and turbulence, with the direct arrivals and sediment reflections having a strong amplitude compared to the turbulence ones. For this reason, The direct arrivals and sediment reflections were suppressed (figure 27). Figure 28 shows the synthetic dataset in the time and F-K domains while figure 29 shows the synthetic dataset with its first and second-order derivatives.

5.2.1 Preconditioning

Two physics-based priors were implemented for the synthetic turbulence dataset, one in the time domain and another in the F-K domain, and are implemented as masks where we expect the signal to belong. For the F-K domain preconditioner, the dispersion is estimated with a triangle shape by using the constant velocity of water (figure 30). For the time domain preconditioner, a constant wave speed is assumed as it is in water. Figure 30 compares the result of the reconstruction with and without the preconditioning mask, with the noise outside the desired

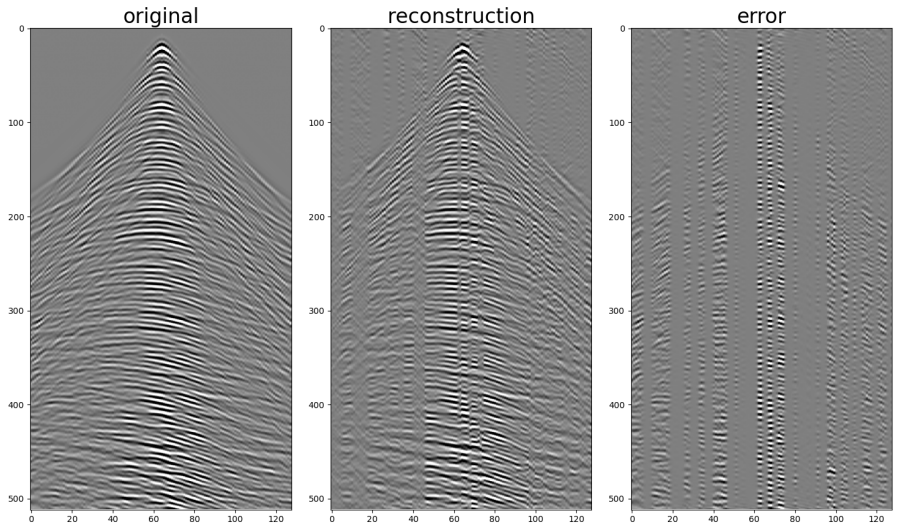

Figure 23: Reconstruction with random subsampling

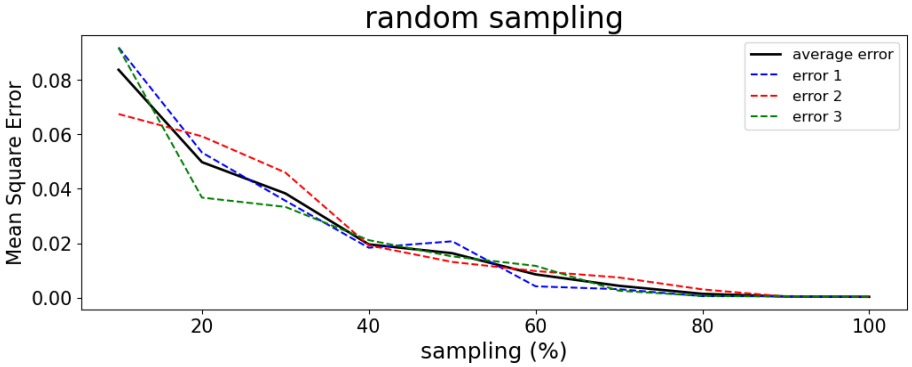

Figure 24: Randomly subsampled data reconstruction errors with different subsampling intervals

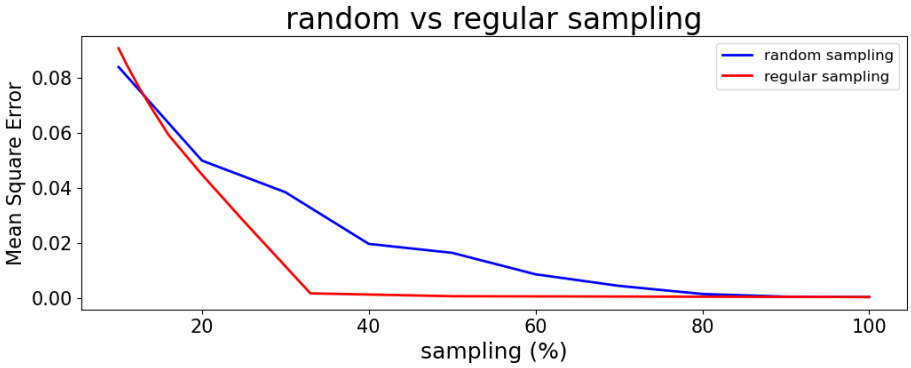

Figure 25: Comparing reconstruction errors for randomly and regularly subsampled data

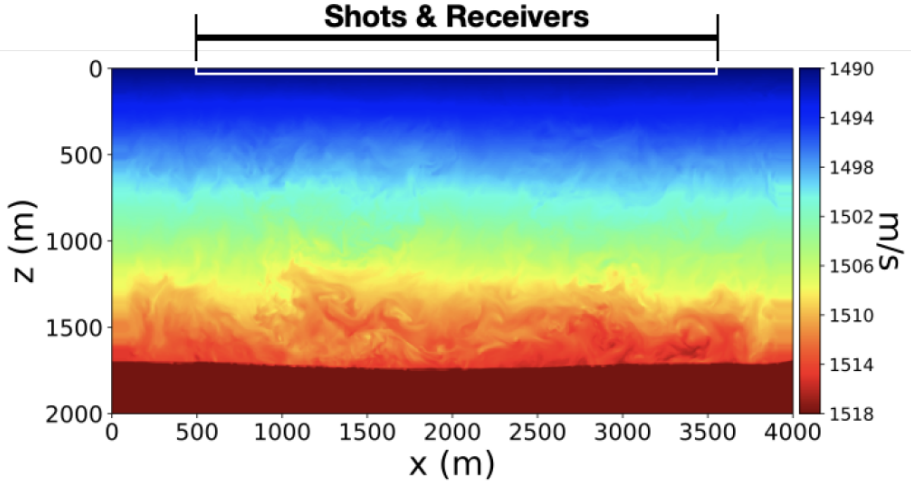

Figure 26: 2D ocean turbulence model [12]

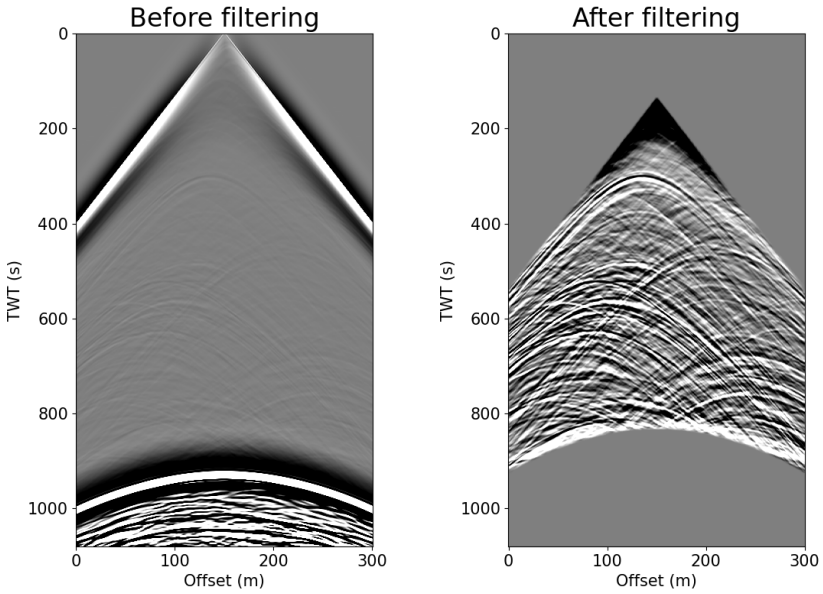

Figure 27: Before (left) and after (right) filtering direct arrivals and sediments reflections

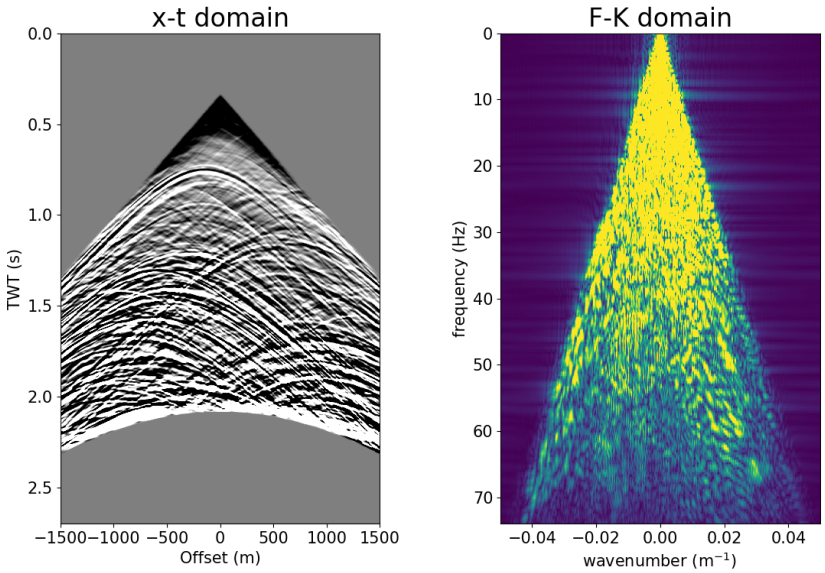

Figure 28: Synthetic data in the time domain (left) and F-K domain (right)

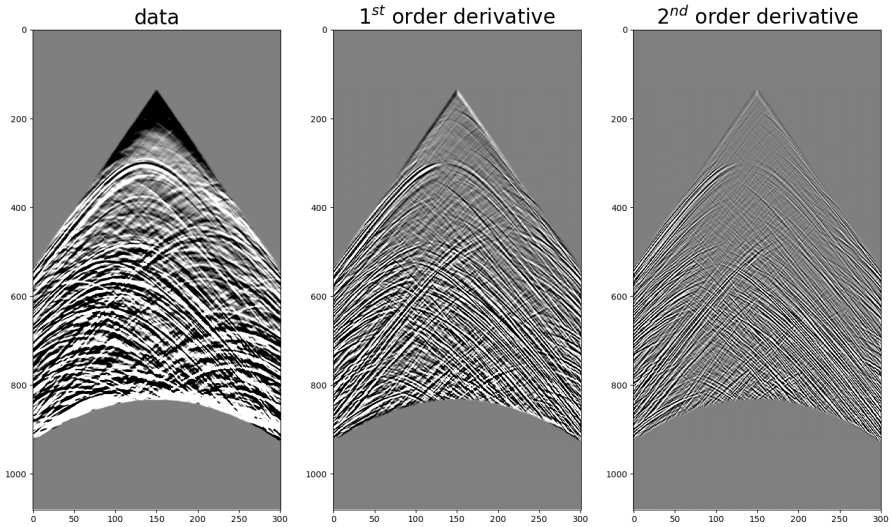

Figure 29: A shot gather with its first and second-order derivatives

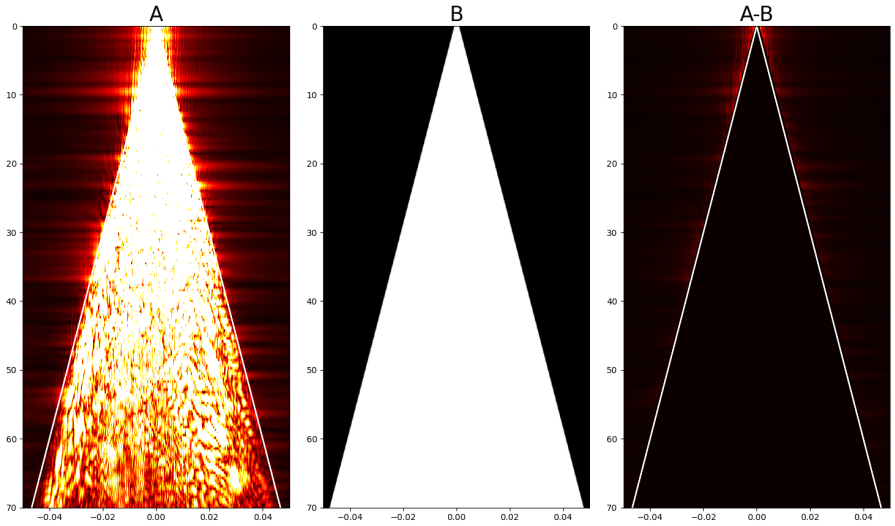

Figure 30: F-K domain preconditioning

area being eliminated. By taking the two preconditioners into account, equation 3 then becomes 11 with P_{xt} and P_{fk} being the space-time and F-K domains preconditioners, respectively.

$$d_{obs} = P_{xt}\ R\ P_{fk}\ F^H\ d_f \tag{11}$$

5.2.2 Regular subsampling

Figures 32 show the regularly subsampled turbulence dataset in the time and F-K domains, respectively. The result of the reconstruction is shown in figure 33. It managed to reconstruct the original data with only a third of the data. In figure 34, we compared different subsampling intervals and their errors, with the reconstruction being faithful when using a third of the data or more.

5.2.3 Random subsampling

Figures 35 show the randomly subsampled turbulence dataset in the time and F-K domains, respectively. The result of the reconstruction is shown in figure 36. This reconstruction is not as good as the regularly subsampled one, mainly because of the large gaps in the data. Figure 37 show reconstruction errors using different subsampling intervals, while figure 38 compares the regular and random errors.

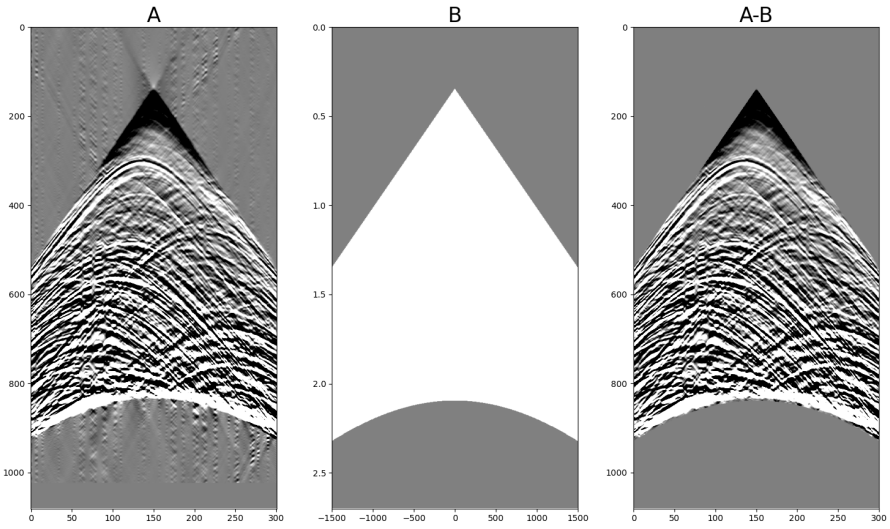

Figure 31: Example before and after time domain preconditioning

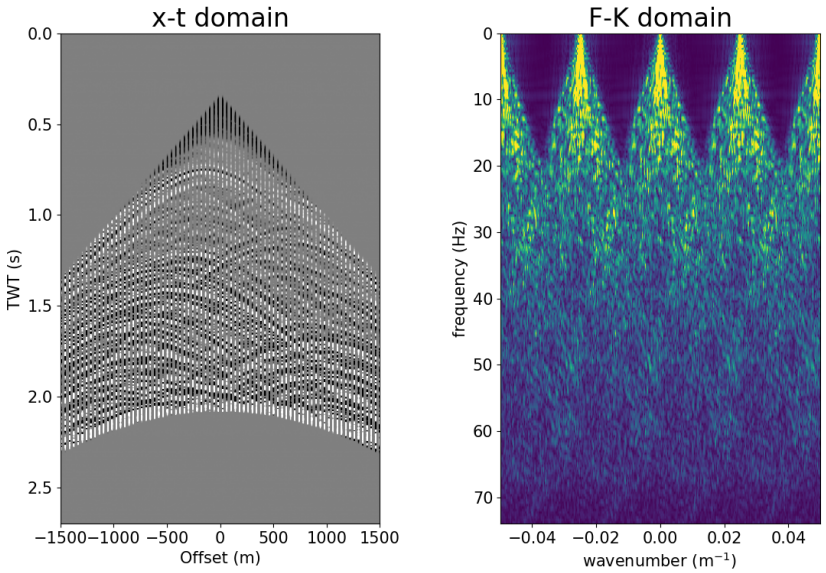

Figure 32: Regular subsampling in the time domain (left) and F-K domain (right)

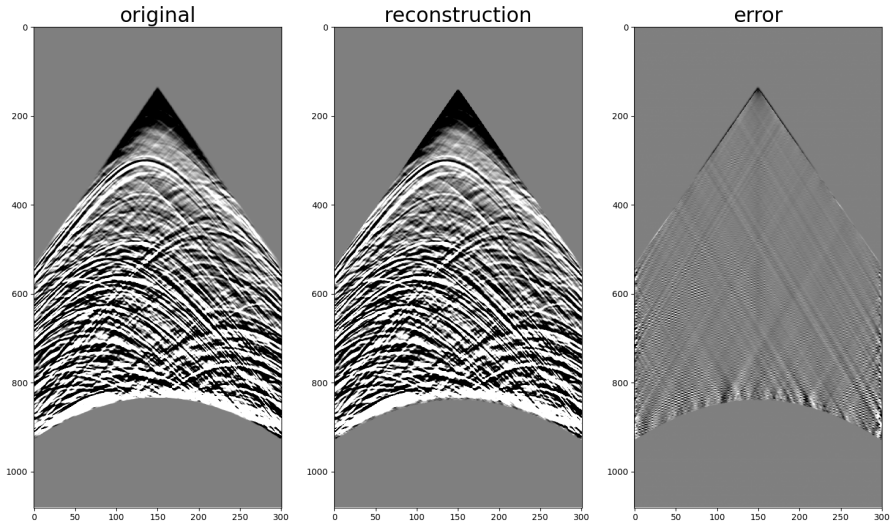

Figure 33: Reconstruction with regular subsampling

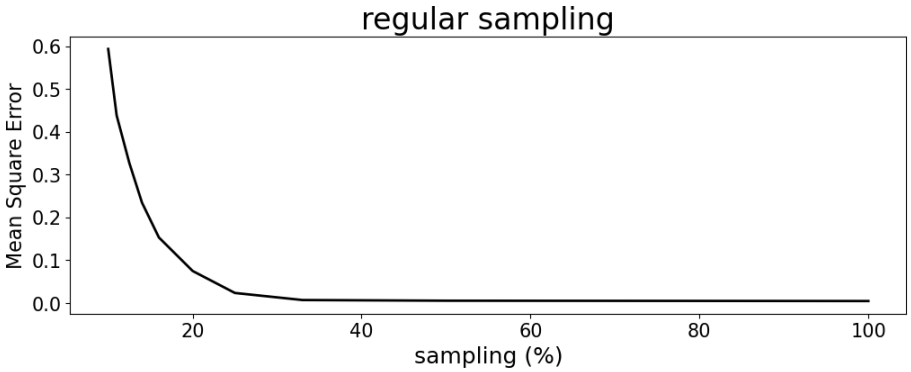

Figure 34: Regularly subsampled data reconstruction errors with different subsampling intervals

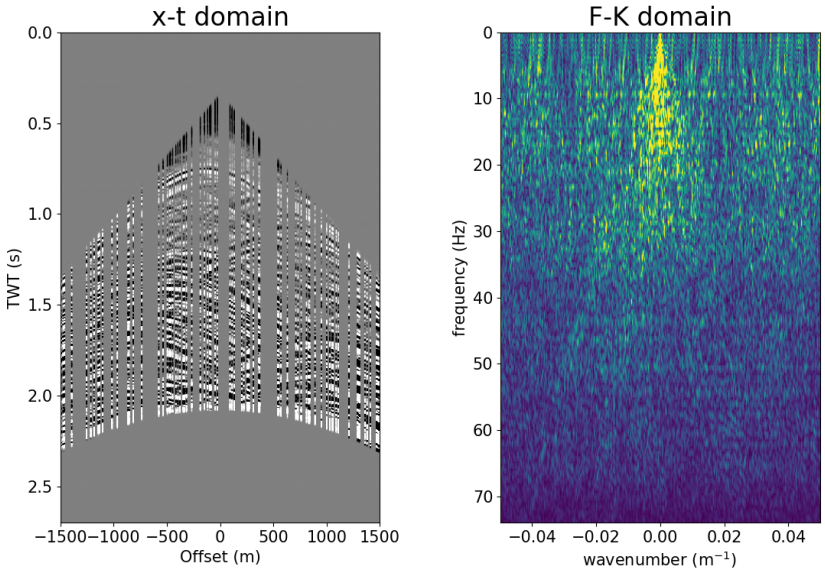

Figure 35: Random subsampling in the time domain (left) and F-K domain (right)

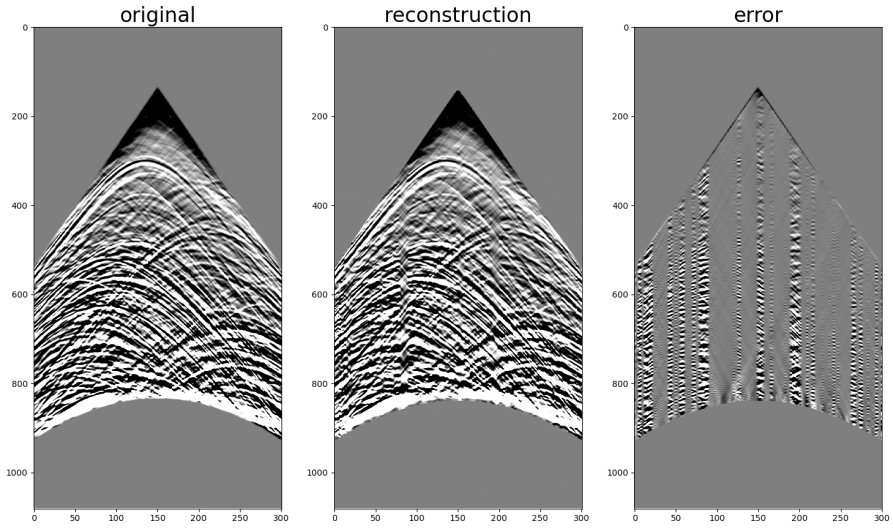

Figure 36: Reconstruction with random subsampling

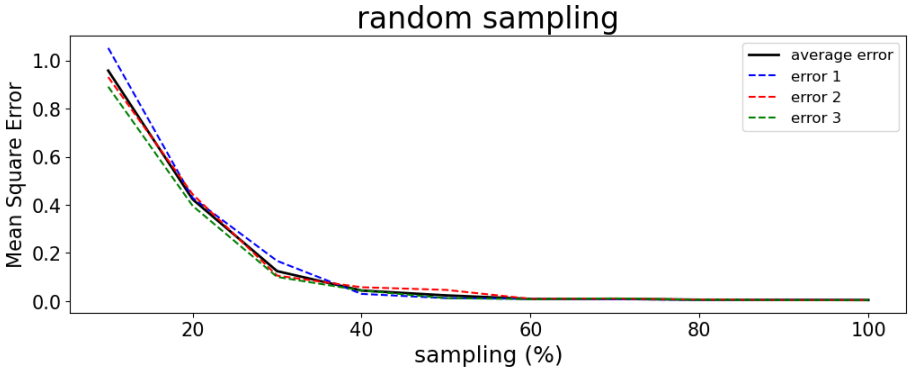

Figure 37: Randomly subsampled data reconstruction errors with different subsampling intervals

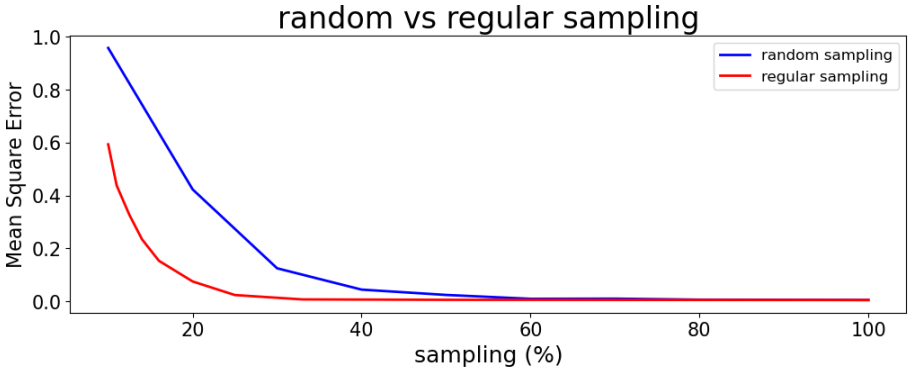

Figure 38: Comparing reconstruction errors for randomly and regularly subsampled data

6 Conclusion

Though highly desired, fully autonomous marine seismic acquisition remains costly and not commercially viable. One way to reduce the cost is by acquiring fewer data, relying thus on fewer and more efficient autonomous platforms. However, this introduces another problem which is missing data. The goal is to minimize the cost while at the same time acquiring as much information (with fewer data) as possible. This can be achieved by using the compressive sensing technique, which can reconstruct signals from under-sampled measurements. Compressive sensing exploits the sparsity of a signal to recover it from fewer samples than that required by the Nyquest-Shannon theorem. The use of first and second-order gradients can further lower this requirement.

Two datasets were used, the Gulf of Suez seismic data and ocean turbulence synthetic data, and subsampled regularly and randomly. The gradients were computed numerically, which is not the same as gradient data acquired in the field. This could produce worse reconstructions as the gradient data acquired in the field is not as clean as the one computed numerically. Thus a more thorough understanding of these reconstructions under realistic noise situations is crucial, though it is beyond the scope of this study. The two datasets were transformed to the F-K domain as it is sparser than the space-time domain, as sparsity is a requirement for the compressive sensing technique.

The two datasets were reconstructed successfully by using only a third of the data. However, The F-K domain is not ideal for this reconstruction as it is not sufficiently sparse for the structure of seismic wavefields. This makes the problem data-dependent, with data sparser in the F-K domain producing better results. There are potentially better domains that could produce better results. One such domain is the curvelet domain, which is known to be a sparser representation of wavefields than the F-K domain.

References

[1] Amir Beck and Marc Teboulle. "A fast iterative shrinkage-thresholding algorithm for linear inverse problems". In: *SIAM journal on imaging sciences* 2.1 (2009), pp. 183–202.

[2] MA Benson et al. "Acquisition using autonomous marine vehicles: Wave glider field test, offshore Abu Dhabi". In: *SPE Middle East Oil & Gas Show and Conference*. OnePetro. 2017.

[3] Steven L Brunton and J Nathan Kutz. *Data-driven science and engineering: Machine learning, dynamical systems, and control*. Cambridge University Press, 2022.

[4] Xander Campman et al. "Sparse seismic wavefield sampling". In: *The Leading Edge* 36.8 (2017), pp. 654–660.

[5] David Chalenski et al. "Rapid autonomous marine 4D (RAM4D): Unmanned time-lapse seismic acquisition". In: *SEG Technical Program Expanded Abstracts 2017*. Society of Exploration Geophysicists, 2017, pp. 5968–5973.

[6] David L Donoho. "Compressed sensing". In: *IEEE Transactions on information theory* 52.4 (2006), pp. 1289–1306.

[7] Youssef Essaouari and Alessio Turetta. "Cooperative underwater mission: Offshore seismic data acquisition using multiple autonomous underwater vehicles". In: *2016 IEEE/OES Autonomous Underwater Vehicles (AUV)*. IEEE. 2016, pp. 435–438.

[8] Nick Moldoveanu et al. "Marine acquisition using autonomous marine vehicles: A field experiment". In: *2014 SEG Annual Meeting*. OnePetro. 2014.

[9] Nick Moldoveanu et al. "Marine seismic acquisition with autonomous marine vehicles towing 3D sensor arrays". In: *The Leading Edge* 36.7 (2017), pp. 558–565.

[10] Iga Pawelec, Michael Wakin, and Paul Sava. "Missing trace reconstruction for 2D land seismic data with randomized sparse sampling". In: *Geophysics* 86.3 (2021), P25–P36.

[11] Matteo Ravasi and Ivan Vasconcelos. "PyLops—A linear-operator Python library for scalable algebra and optimization". In: *SoftwareX* 11 (2020), p. 100361.

[12] J. Ruan. "Compressive Acquisition and Wavefield Reconstruction for Ocean Turbulence Monitoring". MA thesis. Utrecht University, 2019.

[13] Claude E Shannon. "Communication in the presence of noise". In: *Proceedings of the IRE* 37.1 (1949), pp. 10–21.

[14] Constantinos Tsingas, Thierry Brizard, and Abdulaziz Al Muhaidib. "Seafloor seismic acquisition using autonomous underwater vehicles". In: *Geophysical Prospecting* 67.6-Geophysical Instrumentation and Acquisition (2019), pp. 1557–1570.

[15] Chris Walker* and Steve McIntosh. "Autonomous Nodes–The Future of Marine Seismic Data Acquisition?" In: *12th International Congress of the Brazilian Geophysical Society & EXPOGEF, Rio de Janeiro, Brazil, 15–18 August 2011*. Society of Exploration Geophysicists and Brazilian Geophysical Society. 2011, pp. 1–6.